arXiv:1210.4355v1 [cond-mat.str-el] 16 Oct 2012

Realization of a spin-liquid ground state in the high-pressure phase of $Ba_3YIr_2O_9$

Tusharkanti Dey,[1] S. K. Panda,[2] A.V. Mahajan,[1, *] I. Dasgupta,[2, 3]
B. Koteswararao,[4] F. C. Chou,[4] A. A. Omrani,[5] and H. M. Rønnow[5]

[1] *Department of Physics, Indian Institute of Technology Bombay, Powai, Mumbai 400076, India*
[2] *Centre for Advanced Materials, Indian Association for the Cultivation of Science, Jadavpur, Kolkata-700032, India*
[3] *Department of Solid State Physics, Indian Association for the Cultivation of Science, Jadavpur, Kolkata 700032, India*
[4] *Center for Condensed Matter Sciences, National Taiwan University, Taipei 10617, Taiwan*
[5] *Laboratory for Quantum Magnetism, Ecole Polytechnique Federale de Lausanne (EPFL), CH 1015, Switzerland*

Abstract

$Ba_3YIr_2O_9$ crystallizes in a hexagonal structure and transforms into a cubic structure under an applied pressure of 8 GPa at 1273 K. While the ambient pressure (AP) sample undergoes long-range magnetic ordering at ~ 4 K, the high-pressure (HP) synthesized sample does not order down to 2 K as evidenced from our susceptibility, heat capacity and nuclear magnetic resonance (NMR) measurements. Further, for the HP sample, heat capacity measurements demonstrate the presence of a linear term in C/T vs. T^2 in the range of $2-10$ K with $\gamma = 10$ mJ/mol-Ir K^2. The ^{89}Y NMR shift has no temperature (T) dependence in the range of $4-120$ K and spin-lattice relaxation rate varies linearly with T in the range of $8-45$ K (above which it is T-independent). Resistance measurements confirm that both the samples are semiconducting. Our *ab-initio* calculations reveal that strong spin orbit coupling (SOC) plays a crucial role in determining the magnetic and insulating properties of this system in both the phases. We suggest that the cubic (HP) phase of $Ba_3YIr_2O_9$ is a 5d based, gapless, spin-liquid.

PACS numbers: 76.60.-k, 71.15.Mb, 75.70.Tj

The 3d transition metal oxides have been studied extensively to explore novel properties like superconductivity [1, 2], colossal magnetoresistance [3] etc. In these materials, the orbital angular momentum of the valence electrons is largely quenched and a large onsite Coulomb energy often drives the materials to a Mott insulating state. In contrast, for 5d group based materials, this onsite Coulomb energy is smaller by an order of magnitude and one could expect more metallic and less magnetic behavior. However, some 5d Ir-based materials such as $Na_4Ir_3O_8$ [4], Sr_2IrO_4 [5, 6], Na_2IrO_3 [7] etc. are found to be insulators showing exotic magnetic properties. These materials are insulating due to the presence of strong spin-orbit interactions and are often called as spin-orbit driven Mott insulators. Such materials are relatively less explored and expected to offer a promising playground for materials researchers.

To explore this spin-orbit driven physics further, we have recently investigated hexagonal $Ba_3IrTi_2O_9$ and suggested it to be a spin-orbit driven liquid based on a triangular lattice [8]. $Ba_3YIr_2O_9$ has a similar chemical formula and it crystallizes in the hexagonal structure (P6$_3$/mmc) with Ir-Ir structural dimers arranged in an edge shared triangular fashion [9]. Since all the Ir are equivalent, they should have a fractional oxidation state of +4.5 in a simple ionic picture. This should presumably lead to metallic behavior in sharp contrast to the insulating behavior seen in resistivity measurements. In spite of the triangular lattice being frustrated, Doi *et al.* [9] reported magnetic ordering in the above compound at ~ 4 K. It is likely that there is significant spin-orbit coupling in $Ba_3YIr_2O_9$ which therefore warrants a deeper investigation for possible evidence of an exotic ground state. In a similar system $Ba_3NiSb_2O_9$, the ambient pressure sample orders at 13.5 K but its structure changes when exposed under high pressure and it has been proposed to become a spin liquid [10]. It would therefore be interesting to explore $Ba_3YIr_2O_9$ under high pressure to see if any change in crystal structure and hence in magnetic properties takes place.

Herein we report x-ray diffracion, magnetization, heat capacity and ^{89}Y NMR measurements accompanied by first-principles electronic structure calculations for both ambient (AP) and high (HP) pressure phases of $Ba_3YIr_2O_9$ with focus on the HP phase. The AP sample is hexagonal, insulating and orders at ~ 4 K as reported earlier. On the other hand, the HP sample has a cubic structure, exhibits a Curie susceptibility but does not order down to 2 K. More specifically, the HP sample is semiconducting but has a metal-like linear heat capacity coefficient $\gamma = 10$ mJ/mol-Ir K^2. The ^{89}Y NMR shift is independent of temperature T below 120 K and the ^{89}Y NMR spin-lattice relaxation rate crosses over from T-independent behavior at high temperature to a linear T-dependence below about 45 K. These results point to the existence of low-energy excitations at low-temperatures. In the absence of metallic behavior in the resistivity, the low-T data suggest the formation of an exotic ground state, possibly a gapless spin-liquid state. The electronic structure calculations reveal the important role of spin-orbit coupling for the description of the insulating state in both the phases. Together these results establish a new spin-orbit driven Mott-Hubbard insulator.

We have prepared polycrystalline sample of $Ba_3YIr_2O_9$ by solid state reaction method as detailed in Ref. [9]. Further, the AP sample was treated under 8 GPa pressure

---

[*] Email:mahajan@phy.iitb.ac.in

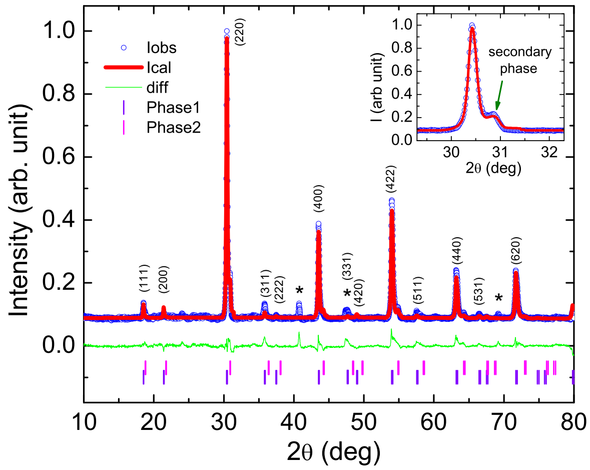

Figure 1: X-ray diffraction pattern of the HP phase of $Ba_3YIr_2O_9$ sample is shown along with a two phase refinement with space group Fm-3m. The (hkl) positions are also indicated. A 5% impurity phase of ureacted Ir is found. The peaks corresponding to Ir are marked with (*). The main peak of the primary phase is shown in the inset.

at 1273 K for 30 min to get the HP sample. Due to the small size of the HP cell, only about 150 mg of sample was obtained.

Our XRD analysis confirmed that the AP sample was formed in a hexagonal structure ($P6_3/mmc$) as reported earlier [9] but after high-pressure treatment the structure changed to a cubic double perovskite ($Ba_2MM'O_6$) phase with space group Fm-3m. It is relevant to mention that $Ba_3NiSb_2O_9$ was also reported to transform from a hexagonal ($P6_3/mmc$) to cubic (Fm-3m) phase when treated under 9 GPa pressure at 1273 K for 30 min [10]. In the XRD pattern (Fig. 1) of the HP phase, a few extra peaks (marked as *) are present which are identified as due to unreacted Ir and account for about 5% of the contribution. Also, all the major peaks have a shoulder on the right side. These shoulders possibly arise from a double perovskite phase with a slightly different cell parameter. Accordingly, a two-phase Rietveld refinement (Fig. 1) performed with our XRD data yields lattice parameter $a = 8.3248$Å for the primary phase and $a' = 8.202$Å for the secondary phase (about 10% content). Refinement with a cubic perovskite structure (chemical formula $Ba(Y_{1/3}Ir_{2/3})O_3$) with approximately half the lattice parameter of the double perovskite (chemical formula $Ba_2Ir(Y_{2/3}Ir_{1/3})O_6$) did not give satisfactory results. We find that an ordered arrangement of IrO_6 and $Y_{2/3}Ir_{1/3}O_6$ octahedra form the cubic double perovskite $Ba_2Ir(Y_{2/3}Ir_{1/3})O_6$ structure of the HP phase (shown in Fig. SM-1 of Supplemental Material (SM) [11]). We note that every Y will have 6 Ir as its nearest neighbors while as next nearest neighbors it will have 33% Ir and 67% Y.

Inset of Fig. 2 shows the magnetic susceptibility of the AP as well as HP samples measured as a function of T in a field 5 kOe. For the AP sample, magnetic susceptibility shows a kink at ~ 4 K indicative of a long range magnetic ordering as reported earlier [9]. Our calculations based on GGA+U+SOC, pertaining to the AP sample, suggest that among the calculated structures, the one with ferromagnetic intra-dimer coupling and an antiferromagnetic inter-dimer coupling (AFM2) has the lowest energy (see SM [11]). Susceptibility data of the AP sample could be fitted to the Curie law in the temperature range $30 - 300$ K which yields a T-independent susceptibility $\chi_0 = 3.8 \times 10^{-4}\,\mathrm{cm^3/mol\ Ir}$ and a Curie constant $C = 0.0125\,\mathrm{cm^3K/mol\ Ir}$. Below about 30 K, the susceptibility deviates from Curie behavior due to building up of magnetic correlations. For the HP sample, no anomaly indicative of a magnetic ordering was seen down to 2 K nor was there any ZFC-FC splitting observed. Data for the HP sample could be fitted to the CW law in almost the whole temperature range resulting in the parameters $\chi_0 = 3.9 \times 10^{-4}\,\mathrm{cm^3/mol\ Ir}$, $C = 0.0045\,\mathrm{cm^3K/mol\ Ir}$ and $\theta = -1.6$ K. The small θ found for the HP sample in the full temperature range indicates the weakness of magnetic interactions. The C value for the AP sample is nearly a factor of 30 smaller than for isolated $S = 1/2$ magnetic moments ($0.375\,\mathrm{cm^3/mol}$). For the HP sample, the C value is smaller by a further factor of 3 compared to its AP counterpart while the χ_0 is nearly unchanged. The absence of long-range order in the HP structure is also anticipated by our electronic structure calculations which find various magnetic structures to be degenerate (see SM [11]). Considering $\chi_0 = \chi_{core} + \chi_{vv}$, where χ_{core} for our sample composition is $-1.37 \times 10^{-4}\,\mathrm{cm^3/mol\ Ir}$, we get $\chi_{vv} = 5.3 \times 10^{-4}\,\mathrm{cm^3/mol\ Ir}$. This is nearly within the range ($1 \times 10^{-4} - 5 \times 10^{-4}\,\mathrm{cm^3/mol\ Ir}$) of χ_{vv} observed in different Ir-based insulating oxides [7, 12]. Absence of a χ_{Pauli} term suggests the sample is insulating.

The low-temperature heat capacity can often throw light on the presence of low-energy excitations in the material. If one is able to separate out the phonon contribution, the residual contribution should represent the electronic part which is generally of interest. Whereas in the AP sample a clear anomaly at about 4K is seen in the heat capacity (see Fig. 2) which reflects long-range order, the anomaly goes away in the HP sample. This indicates that magnetic ordering has been suppressed by the application of pressure. It is further interesting to note that for the HP sample below about 10 K, C_P/T vs T^2 is linear (see Fig. 2) and gives a non-zero Sommerfeld coefficient $\gamma = 10\,\mathrm{mJ/mole\text{-}Ir\,K^2}$ and $\beta = 0.44\,\mathrm{mJ/mol\text{-}Ir\,K^4}$. Although this γ value is typical of metallic materials, our resistance measurement on single crystals show semiconductor like behavior (see SM [11]). These results could imply the exotic possibility of the absence of charge excitations while spin-excitations are present. In such a scenario, one can interpret the linear contribution to the low-T heat capacity as coming from excitations from a spinon Fermi surface as might happen in a gapless spin-liquid.

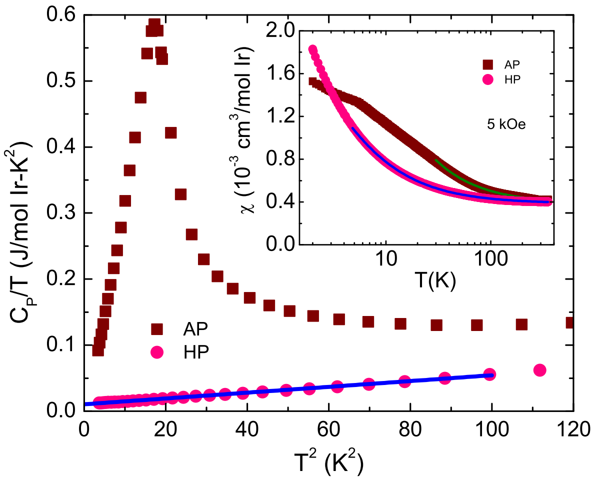

Figure 2: C_P/T vs T^2 is shown for the AP and HP samples. The solid line is a linear fit to data for the HP sample. Inset: Magnetic susceptibility of AP and HP samples measured in a 5kOe field and their fitting (solid lines) with Curie-Weiss law.

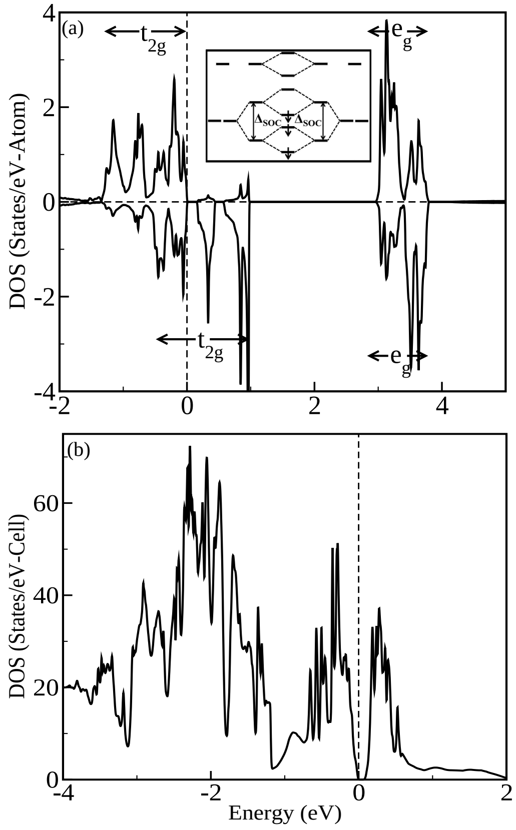

Figure 3: PDOS of Ir-d states within GGA+U+SOC for (a) AP and (b) HP phase. Schematic to explain the insulating behavior of AP phase is shown in the inset.

Before we present further evidence of such non-standard behavior of the HP phase in other measurements we shall discuss the origin of the unusual insulating state in both the AP as well as HP samples where Ir is expected to have a fractional oxidation state of +4.5. To understand this issue we have performed electronic structure calculations within local (spin) density approximation with generalized gradient correction (GGA) of Perdew-Burke-Ernzerhof including Hubbard U and spin orbit coupling (SOC) (for details see SM [11]). In Fig 3(a) we have displayed the partial density of states of Ir-d states in the AP phase for the AFM2 structure. The DOS reveal that the system is insulating. In the following we shall argue that in contrast to other irridates, in addition to SOC and Hubbard U the strong intra-dimer coupling plays a key role for the system to be insulating. The DOS reveal that the exchange splitting is much smaller compared to the crystal field splitting. So Ir ($d^{4.5}$) remains in the low spin state. As a consequence majority t_{2g} states are completely occupied and the remaining 1.5 electrons/Ir are accommodated to the minority spin channel. The origin of the gap in the minority spin channel is schematically illustrated in the inset of Fig 3(a) where we have only shown the Ir-t_{2g} states in the minority spin channel for an Ir-Ir dimer. The threefold degeneracy of the t_{2g} states is lifted by the distortion of IrO_6 octahedron and by SOC (see SM [11] for details). This is however not enough to open up a gap in the minority spin channel with 1.5 electron/Ir. Interestingly a strong intra-dimer coupling produces a set of bonding and anti-bonding states shown in the middle panel of the inset of Fig. 3(a). The three electrons available per dimer will occupy the states and can open up a gap at the Fermi level provided the bandwidth is smaller than the splitting due to dimerization. In such a situation, a small but finite Hubbard U (U = 3 eV) promotes an insulating state by increasing the separation between the occupied and unoccupied states. In Fig. 3(b) we have shown the total non-spin polarized DOS for a model system $Ba_2Ir(Y_{3/4}Ir_{1/4})O_6$ which is very close to the experimentally synthesized $Ba_2Ir(Y_{2/3}Ir_{1/3})O_6$ obtained in the HP cubic phase. Our calculations reveal strong spin-orbit coupling and difference in the filling of the t_{2g} levels for Ir and Ir_Y (i.e. Ir at the Y site) are responsible for promoting the insulating state.

Having established the insulating state for the AP and HP phases, we looked for signs of novel magnetic behavior using the ^{89}Y NMR local probe via spectra and spin-lattice relaxation rate measurements (which probe the low-energy excitations) on both the AP sample and the HP one (a mere 150 mg). Here, we focus on the data below about 120 K which is relevant to the theme of this paper. The spectrum of the AP sample shifts negatively with decreasing temperature (inset (a) of Fig. 4), in line with the Curie-like susceptibility and a negative hyperfine coupling constant. The linewidth too, increases with decreasing temperature and tends to diverge at ∼ 4 K (inset (b) of Fig. 4) as a signature of the onset of long-

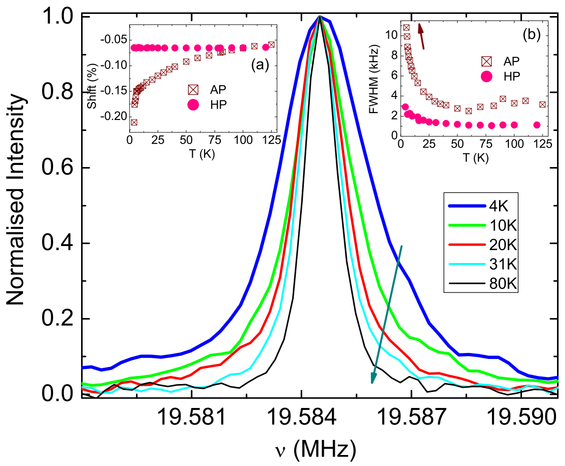

Figure 4: ^{89}Y NMR spectra at different temperatures for the HP sample are shown. The arrow indicates measurement temperature in increasing order. Inset: (a) and (b) show the Shift and FWHM, respectively, of the AP sample as well as the HP sample as functions of temperature. The arrow in the inset (b) indicates that FWHM for the AP sample goes much higher at low temperature (∼ 40kHz at 4K).

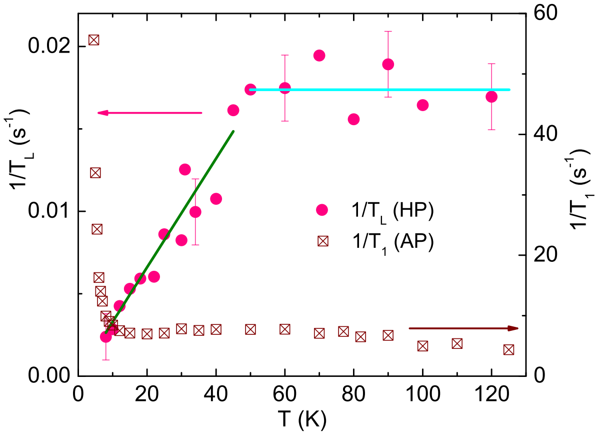

Figure 5: $1/T_L$ for the HP sample is shown on the left axis. $1/T_L$ increases linearly with T in the range $8 - 45$ K. Above 45 K, $1/T_L$ is almost independent of T. Solid lines are guides to the eye. On the right axis, $1/T_1$ for the AP sample is shown.

range order. A corresponding signature is also seen in the divergence of the ^{89}Y NMR $1/T_1$ for the AP sample. In contrast, the spectra for the HP sample (shown in Fig. 4) are narrower and the width increases only slightly with decreasing temperature without any divergence. This would seem to be in tune with the much weaker Curie-term and the lack of magnetic order seen in the susceptibility. Somewhat surprisingly, though, the ^{89}Y NMR shift for the HP sample is T-independent below 120 K. The ^{89}Y NMR relaxation rate (Fig. 5) for the HP sample is T-independent at high-T as might be expected in a paramagnet insulator but crosses over to a linear variation below about 45 K (the rate corresponding to the longer T_1 component ($1/T_L$) is plotted here; (see SM [11] for details). The constancy of the ^{89}Y NMR shift for the HP sample coupled with the Curie-like susceptibility variation in the same temperature range suggest one of the two things, (i) a very weak hyperfine coupling results in an insensitivity to the small susceptibility variation (this is in accord with the long T_1) or (ii) the low-T increase of the susceptibility is of extrinsic origin and that the intrinsic spin susceptibility saturates as one decreases temperature and remains constant below 120K.

Our susceptibility, resistivity data and electronic structure calculations support the paramagnetic insulator picture but once again, a non-zero γ and crossover in $1/T_1$ data run counter to this idea. On the other hand, the linear behavior in C_P/T vs T^2 with a non-zero intercept and the linear variation of $1/T_1$ with T, inspite of insulating behavior point to a gapless spin liquid state. In this context it is relevant to point out NMR results on other spin liquid systems. For the 5d-based spin liquid system $Na_4Ir_3O_8$, ^{23}Na NMR by Takagi *et al.* [13] find a negligible temperature dependence of shift below about 100 K since the susceptibility was saturated. In this case the ^{23}Na $1/T_1$ was constant above 200 K below which it followed a power law with power 1 in the range $2 - 10$ K and with power 2.5 in the temperature range $100 - 200$ K. They attributed this low-temperature linear behavior to low lying spin excitations. Itou *et al.* [14] also found almost no temperature dependence of shift in their ^{13}C NMR data down to 18.7 mK on the organic system $EtMe_3Sb[Pd(dmit)_2]_2$ with a spin liquid ground state while $1/T_1$ was found to be constant in some range above 1 K and varied as T^2 below 1 K. In the organic spin liquid system κ-(BEDT-TTF)$_2$Cu$_2$(CN)$_3$, Shimizu *et al.* [15] found no change in ^{1}H NMR spectral position from 36.1 K down to 32 mK while $1/T_1$ followed a power law at low-temperature, from which the authors concluded that the ground state has gapless low lying spin excitations. Our NMR data are qualitatively similar to the cases listed above, providing further justification for the spin liquid state at low T. It is worth mentioning that another B site ordered double perovskite Ba_2YMoO_6 was reported to have an exotic valence bond glass state [16] or a collective (gapped) spin-singlet state [17].

In conclusion, a strong SOC plays a crucial role in the insulating behavior of both AP and HP samples. The magnetic behavior of the AP and HP phases are markedly different. We have also shown that the AP sample orders magnetically at ∼ 4 K. The ordering vanishes and the magnetism becomes very weak in the case of the HP sample. For the HP sample, the linear term in heat capacity and linear temperature dependence of relaxation rate could be arising from the excitations out of the spinon Fermi surface of a spin liquid with very weak moments.

From our low-T data, we suggest that the HP phase of $Ba_3YIr_2O_9$ is a $5d$-based, gapless, spin liquid.

We thank Department of Science and Technology, Govt. of India for financial support. This work was partially supported by Swiss National Science Foundation and the Indo Swiss Joint Research Programme. FCC acknowledges the support from National Science Council of Taiwan. We thank B. H. Chen for his help in preparation of the HP phase sample.

---

[1] J. G. Bednorz and K. A. Mueller, Z. Phys. B: Condens. Matter **64**, 189 (1986)

[2] Y. Kamihara, T. Watanabe, M. Hirano, and H. Hosono, J. Am. Chem. Soc. **130**, 3296 (2008)

[3] Y. Tokura, Colossal Magnetoresistive Oxides, Gordon & Breach Science, New York, (2000)

[4] Y. Okamoto, M. Nohara, H. Aruga-Katori, and H. Takagi, Phys. Rev. Lett. **99**, 137207 (2007)

[5] B. J. Kim, H. Jin, S. J. Moon, J.-Y. Kim, B.-G. Park, C. S. Leem, J. Yu, T. W. Noh, C. Kim, S.-J. Oh, J.-H. Park, V. Durairaj, G. Cao, and E. Rotenberg, Phys. Rev. Lett. **101**, 076402 (2008)

[6] B. J. Kim, H. Ohsumi, T. Komesu, S. Sakai, T. Morita, H. Takagi, and T. Arima, Science **323**, 1329 (2009)

[7] Y. Singh and P. Gegenwart, Phys. Rev. B **82**, 064412 (2010)

[8] T. Dey, A.V. Mahajan, P. Khuntia, M. Baenitz, B. Koteswararao, and F. C. Chou, arXiv:1210.3137, (to be published in Phys. Rev. B (R))

[9] Y. Doi and Y. Hinatsu, J. Phys.: Condens. Matter **16**, 2849 (2004)

[10] J. G. Cheng, G. Li, L. Balicas, J. S. Zhou, J. B. Goodenough, Cenke Xu, and H. D. Zhou, Phys. Rev. Lett. **107**, 197204 (2011)

[11] See Supplemental Material below

[12] T. Sakamoto, Y. Doi, and Y. Hinatsu, J. Solid State Chem. **179**, 2595 (2006)

[13] See http://online.itp.ucsb.edu/online/motterials07/takagi/pdf/Takagi_Motterials_KITP.pdf

[14] T. Itou, K. Yamashita, M. Nishiyama, A. Oyamada, S. Maegawa, K. Kubo, and R. Kato, Phys. Rev. B **84**, 094405 (2011)

[15] Y. Shimizu, K. Miyagawa, K. Kanoda, M. Maesato, and G. Saito, Phys. Rev. Lett. **91**, 107001 (2003)

[16] M. A. de Vries, A. C. Mclaughlin, and J.-W. G. Bos, Phys. Rev. Lett. **104**, 177202 (2010)

[17] T. Aharen *et al.*, Phys. Rev. B **81**, 224409 (2010)

Supplemental material for “Realization of a spin-liquid ground state in the high-pressure phase of $Ba_3YIr_2O_9$”

****

I. DETAILS OF EXPERIMENTS

Powder x-ray diffraction (XRD) measurements were performed at room temperature with Cu K_α radiation ($\lambda = 1.54182$Å) in a PANalytical X’Pert PRO diffractometer using Si for calibration. Analysis of XRD data for the HP sample reveals that the sample is transformed to a cubic double perovskite structure as shown in Fig. SM-1. The red octahedra represent IrO_6 and among the violet octahedra, 1/3 are IrO_6 and 2/3 are YO_6.

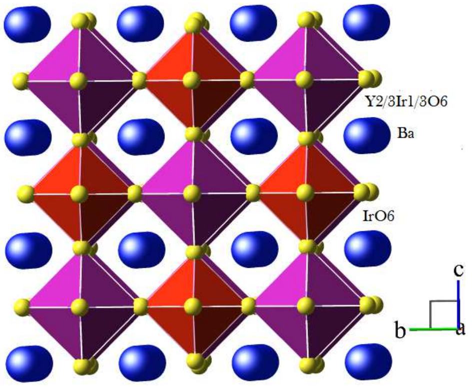

Figure SM-1: The crystal structure of the high pressure synthesized cubic phase is shown. The blue and yellow atoms represent Ba and O, respectively. The red octahedra are IrO_6 octahedra while the violet octahedra contain Ir or Y at their centres.

Magnetization measurements (shown in the main paper) were carried out in the temperature range $2-400\,$K and field range $0-7\,$T using a Quantum Design SQUID VSM. Heat capacity measurements were performed using the heat capacity attachment of a Quantum Design Physical Properties Measurement System (PPMS) in the temperature range $1.8-300\,$K and field range $0-9\,$T.

We have measured resistance on small single crystals [600μm$\times150\mu$m$\times100\mu$m (approx.)] (from the same batch on which other measurements are done) for both AP and HP samples using the four probe technique. The temperature dependence of resistance for both the samples is semiconductor-like (Fig. SM-2).

For ^{89}Y NMR measurements, a Tecmag pulse spectrometer and a fixed magnetic field 93.954 kOe obtained inside a room-temperature-bore Varian superconducting magnet were used. Variable temperature was obtained with the help of an Oxford cryostat and accessories. The ^{89}Y nucleus has spin $I = 1/2$ (100% natural abundance) and gyromagnetic ratio $\gamma/2\pi = 2.08583\,$MHz/T.

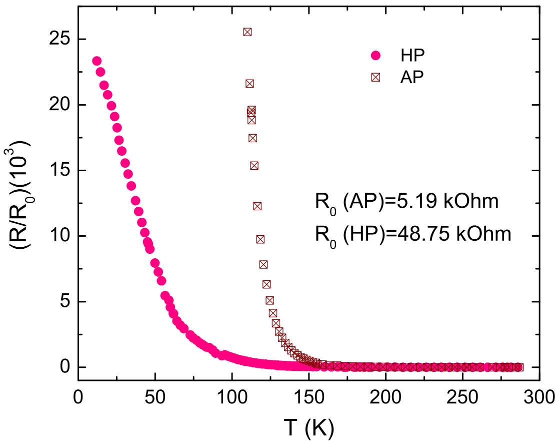

Figure SM-2: Normalised resistance of both AP and HP sample as a function of temperature. R_0 is the resistance at room temperature and the values are mentioned in the figure.

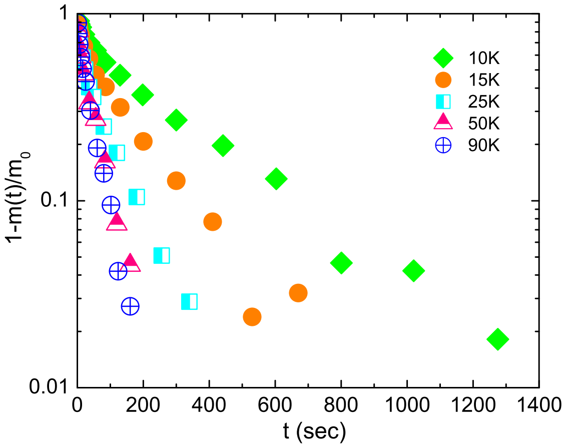

Figure SM-3: Recovery of the ^{89}Y longitudinal nuclear magnetization after a saturating pulse is shown for the HP sample at a few temperatures.

We have measured spin-lattice relaxation rate ($1/T_1$) using a standard saturation recovery method following a $\pi/2 - t - (\pi/2 - \pi)$ pulse sequence in the temperature range $4-300\,$K for the AP sample and $8-120\,$K for the HP sample. For the AP sample, nuclear magnetisation recoveries are single exponential as expected for $I = 1/2$ nucleus. Relaxation time (T_1) for the AP sample varies from about 10 ms to about 400 ms as a function of temperature. For the HP sample the nuclear magnetisation recovery after a saturating pulse has an initial short component followed by a longer component. A few representative recoveries are shown in the Fig. SM-3. We have

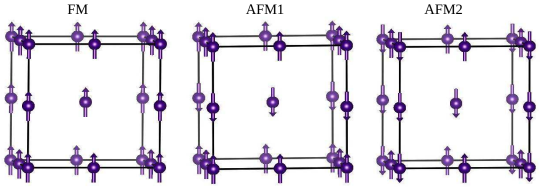

Figure SM-4: Three possible magnetic ordering for the HP phase.

fitted the recoveries with the formula

$$1 - m(t)/m_0 = A[Bexp(-t/T_L) + (1-B)exp(-t/T_S)] \quad (1)$$

where T_L and T_S are the longer and shorter components of T_1, respectively, and B is ~ 0.7. T_L varies from about 40 s at 100 K to about 400 s at 8 K. Below 8 K, T_L becomes even longer though we did not take detailed data. The major differences of T_1 between the AP and HP sample are, (i) T_1 is almost three orders of magnitude higher for the HP sample compared to the AP sample and (ii) relaxation rate ($1/T_1$) increases with decreasing temperature for the AP sample but decreases with decreasing temperature ($T < 45$ K) for the HP sample.

II. DETAILS OF THEORETICAL CALCULATIONS

Density functional theory calculations have been performed using three different methods, namely (a) plane wave based method as implemented in Vienna *ab initio* simulation package (VASP) [1, 2] (b) full potential linearized augmented plane wave method (FP-LAPW) [3] and (c) N$^{\text{th}}$ order muffin-tin orbital (NMTO) method [4]. To begin with, we have checked the relative stability of various magnetic configurations using VASP. The calculations were performed within local (spin) density approximation (LSDA) with generalized gradient correction (GGA) of Perdew-Burke-Ernzerhof [5] including Hubbard U and spin-orbit coupling SOC. The kinetic energy cut off of the plane wave basis was chosen to be 500 eV. Brillouin-Zone integration have been performed using $10\times10\times4$ k-mesh for the AP phase and $10\times10\times10$ k-mesh for the HP phase. In order to calculate the DOS, the partial DOS, the orbital and magnetic moment corresponding to the lowest energy state, we have employed the all-electron FP-LAPW method. We have taken the value of on-site Coulomb repulsion (U) as 3 eV to understand the effect of correlations. Finally to extract the tight binding parameters and to understand the crystal field splitting, we have constructed low energy model Hamiltonian using the downfolding procedure as implemented in the NMTO method [4].

We have first investigated whether magnetism can be stabilized in the AP and the HP phase using GGA+U+SOC calculations in the framework of LAPW method. For the AP phase, we have considered four different magnetic configurations, namely FM (both the intra and inter dimer couplings are ferromagnetic), AFM1 (both the intra and inter dimer couplings are antiferromagnetic), AFM2 (intra dimer coupling is ferromagnetic and inter dimer coupling is antiferromagnetic), and AFM3 (intra dimer coupling is antiferromagnetic and inter dimer coupling is ferromagnetic).

Table SM-1: Energy of various magnetic state with respect to the FM state in meV/Ir.

Configurations	FM	AFM1	AFM2	AFM3
GGA+U+SOC	0.0	34.55	-9.16	29.20

Our calculations as summarized in Table SM-1 reveal that AFM2 state has the lowest energy. To understand the microscopic origin of the insulating behavior (see Fig. 3(a) of the main paper), we performed NMTO downfolding calculations and constructed a Ir-d only low-energy Hamiltonian by integrating out the high degrees of freedom other than Ir-d for the AP hexagonal phase. Diagonalization of the on-site block give the following eigen states with energies -4.26, -4.26, -4.11, -0.48 and -0.48 eV respectively.

$$\begin{aligned}
|1\rangle &= -0.8135|xy\rangle + 0.5815|yz\rangle \\
|2\rangle &= -0.5815|xz\rangle - 0.8135|x^2-y^2\rangle \\
|3\rangle &= |z^2\rangle \\
|4\rangle &= -0.5815|xy\rangle - 0.8135|yz\rangle \\
|5\rangle &= -0.8135|xz\rangle + 0.5815|x^2-y^2\rangle
\end{aligned}$$

Clearly, the first three states form the t$_{2g}$ manifold and the other two form the e$_g$ manifold. Because of the distortion in the octahedra, the three fold degeneracy of the t$_{2g}$ block is lifted. The t$_{2g}$-e$_g$ crystal field splitting is quite large (~ 3.6 eV) which is also visible in the PDOS (see Fig 3(a) of the main paper). As the exchange splitting is much smaller compared to the crystal field splitting, Ir (d$^{4.5}$) remain in the low spin state. The origin of this gap can be understood by ignoring the spin mixing term of the SOC Hamiltonian and only concentrating on the minority t$_{2g}$ bands. With this simplification, we can diagonalize the SOC Hamiltonian, having matrix element $\langle i|\lambda\ \hat{\text{L}}.\hat{\text{S}}|j\rangle$, $(i, j = |1\rangle, |2\rangle, |3\rangle)$ and find that the degeneracy of $|1\rangle$ and $|2\rangle$ is lifted upon inclusion of SOC, while $|3\rangle$ remains unperturbed. This is schematically illustrated for a Ir dimer in the inset of Fig. 3(a) of the main paper. Our NMTO downfolding calculation also reveal that the hopping strength between various t$_{2g}$ orbitals of the two Ir's which form the structural dimer is strong. Therefore these orbitals will interact strongly with each other and form six non-degenerate states (see inset of Fig. 3(a) of the main paper). The two Ir will have total three electrons in the minority channel and will occupy three states among the six non-degenerate levels leading to an insulator as explained in the letter.

For the HP cubic phase, to keep our computation less expensive, we have simulated $Ba_2Ir(Y_{3/4}Ir_{1/4})O_6$ which is very close to the experimentally synthesized $Ba_2Ir(Y_{2/3}Ir_{1/3})O_6$ system. Our calculations find all the magnetic configurations considered here (see Fig. SM-4) to be degenerate.

---

[1] G. Kresse and J. Hafner, Phys. Rev. B **47**, 558 (1993)

[2] G. Kresse and J. Furthmüller, Phys. Rev. B **54**, 11169 (1996)

[3] P. Blaha, K. Schwarz, P. I. Sorantin, and S. B. Trickey, Comput. Phys. Commun. **59**, 399 (1990)

[4] O. K. Andersen and T. Saha-Dasgupta, Phys. Rev. B **62**, 16219(R) (2000)

[5] J. P. Perdew, K. Burke, and M. Ernzerhof, Phys. Rev. Lett. **77**, 3865 (1996)